Deterministic versus Stochastic Optimization for Joint Path Planning and Dynamic Time Splitting in Multiple-UAV-Cached IoT Networks

Trinh Van Chien, Dinh Thanh Tung, Waqas Khalid, Ngo Cong Dung, Banh Thi Quynh Mai, and Symeon Chatzinotas

***Abstract*—This paper examines wireless-powered Internet of Things (IoT) networks involving multiple unmanned aerial vehicles (UAVs) equipped with backscatter and caching technologies to relay and transmit signals. For data communication and energy harvesting, the source transmits information and power to UAVs using the dynamic time splitting (DTS) method. UAVs use the harvested energy for passive communication (backscattering) and active communication (transmitting information) to the destination. The primary objective is to maximize total throughput by jointly optimizing the DTS ratio, trajectory, and transmission power, leveraging its caching capability. This optimization problem is challenging due to its non-convexity. We therefore propose an efficient alternating algorithm using the block coordinate descent (BCD) method. This algorithm optimizes the DTS ratio, trajectory, and data transmission capacity of each UAV, given the fixed values of the other two parameters. By applying the Karush-Kuhn-Tucker (KKT) conditions, we derive a closed-form expression for the optimal DTS ratio, significantly reducing computation time. The optimal values for the other two parameters are determined using the successive convex approximation (SCA) technique. In order to thoroughly assess the effectiveness of various solutions for the original problem, this paper introduces an approach leveraging a genetic algorithm (GA). The GA in this context employs a one-point crossover method, value mutation, and a rank-based selection mechanism evaluated by fitness values. This comprehensive evaluation not only highlights the capabilities of the GA but also provides a robust comparison framework for the proposed solutions. The findings highlight the significant throughput gains achieved by the proposed approaches.**

***Index Terms*—Unmanned aerial vehicle (UAV), wireless-powered communication, block coordinate descent (BCD), genetic algorithm (GA).**

I. Introduction

Unmanned aerial vehicles (UAVs) have become essential in military, civilian, and commercial domains, supporting surveillance, disaster relief, environmental monitoring, and agriculture [1], [2]. Their ability to access dangerous locations and quickly collect data across large areas enhances operational efficiency [3], [4]. Technological advancements continue to extend UAVs' flight duration, payload capacity, and communication range, positioning them as effective tools in wireless communication. UAVs serve as relay nodes to counteract signal degradation from shadowing or congested base stations (BSs) [5], and as airborne BSs to restore connectivity during disasters when terrestrial BSs are impaired. Compared to portable ground BSs, UAVs offer faster deployment and resilience to infrastructure failures [6]. Nonetheless, increasing UAV operations introduces challenges related to energy usage and memory limitations. Employing technologies such as backscatter and caching helps mitigate these issues by enhancing energy conservation and data handling capabilities. Recent progress in IoT-enabled UAV systems demonstrates that laser-powered backscatter significantly improves energy harvesting for extended missions [7]. Furthermore, integrating backscatter with UAV-assisted mobile edge computing has proven effective in reducing latency and energy consumption in dense IoT environments [8].

Backscatter communication (BackCom) addresses energy efficiency in UAV networks using circuits that operate at micro-Watt (μW) power levels [9], [10], [11]. Efficiency is further improved through optimized UAV flight paths, backscatter device (BD) scheduling, and carrier emitter (CE) management [12]. Although transmission requires minimal power, UAV propulsion remains energy-intensive, reaching hundreds of Watts [13], and limited battery storage imposes operational constraints [14]. As a solution, wireless power transfer (WPT) supports continuous UAV activity across diverse applications [15], [16], [17], [18]. Jayakody *et al.* [19] proposed a self-sustaining UAV system by integrating energy harvesting (EH), WPT, and simultaneous wireless information and power transfer (SWIPT), resolving self-interference in full-duplex transmission. In another study, Yan *et al.* [20] focused on UAV-enabled wireless sensor networks (WSNs), where UAVs harvested energy from base stations to serve multiple WSNs, optimizing total energy acquisition across sensors. Recent advances have also demonstrated UAV-based backscatter systems enabling mobile edge computing for IoT applications with improved computation success rates [21].

Cache memory plays a critical role in reducing latency and easing network congestion by storing frequently accessed content near end users [22], [23]. In UAV networks, onboard caching notably improves response time in areas with difficult terrain or limited infrastructure. Deploying caches at edge UAV nodes not only enhances system efficiency but also addresses latency concerns. Masood *et al.* [24] introduced a content caching scheme for high-altitude platform (HAP)-assisted multi-UAV systems, employing a hierarchical federated learning algorithm to forecast content demand while

Trinh Van Chien, Dinh Thanh Tung, Ngo Cong Dung, and Banh Thi Quynh Mai are with the School of Information and Communication Technology, Hanoi University of Science and Technology, Hanoi 100000, Vietnam (email: chientv@soict.hust.edu.vn). Waqas Khalid is with the Institute of Industrial Technology, Korea University, Sejong 30019, Korea (Email: waqas283@gmail.com, korea.ac.kr). Symeon Chatzinotas is with the with the Interdisciplinary Centre for Security, Reliability and Trust (SnT), University of Luxembourg, 1855 Luxembourg, Luxembourg (e-mail: symeon.chatzinotas@uni.lu).

ensuring user privacy. Meanwhile, Zhang *et al.* [25] designed a UAV-enabled protocol for data dissemination in Vehicle-to-Everything networks that merges proactive caching with cooperative file sharing. Their solution leverages dynamic trajectory scheduling to optimize cache duration and applies relay prioritization with channel prediction to increase sharing performance. A recent study also showed that joint cooperative caching and power control in UAV-enabled IoT vehicular networks significantly improves energy efficiency [26].

Building on previous discussions and highlighting the efficiency of wireless power, caching, and backscatter communication technologies, this study examines a caching-enabled BackCom network with multiple UAVs equipped with SWIPT capabilities. UAVs also cache frequently requested content, reducing the data transmitted from the source for relaying to the destination. In contrast to prior studies in [27], which primarily focus on a single UAV functioning as a transmitter or receiver in 2D space or neglect the optimization of total power, this research addresses a network of UAVs functioning as airborne BDs. These UAVs harvest energy from the RF signals emitted by the source and utilize this energy to reflect the signal toward the destination in a 3D environment, effectively enhancing network efficiency and functionality. In summary, key contributions include:

1) This paper explores a communication network where a source transmits to a destination in the absence of a direct link, necessitating the assistance of UAVs. We propose a novel wireless-powered UAV communication network, incorporating backscatter and cache-assisted technologies. The integration of caching and backscatter significantly reduces power consumption, while the base station supplies energy to the UAV, addressing the sustainability challenges associated with UAV operations.
2) Continuous hovering above the source is infeasible due to UAV movement constraints. The dynamic time splitting (DTS) method is employed, dividing each UAV empowered by backscatter devices (UBD) movement slots into intervals for energy harvesting and data transmission. Hence, DTS ratio, power transmission, and UAV trajectory require careful planning to optimize throughput under energy constraints. The DTS ratio determines harvested energy and data rates, necessitating precise scaling in each time slot.
3) The throughput maximization problem includes constraints on UAV flying time, speed, trajectory, power, and DTS ratio. To address its non-convex nature, the problem is divided into three sub-problems: optimizing DTS ratio for a fixed trajectory and power, optimizing trajectory for a given DTS ratio, and optimizing total power using results from earlier steps. Closed-form DTS solutions, derived via KKT conditions, reduce computational complexity. Trajectory and power optimizations are solved using the successive convex approximation (SCA) technique. A three-layer alternating algorithm based on block coordinate descent (BCD) integrates these solutions.
4) A GA-based approach is introduced to evaluate solutions for the original problem. It employs single-point crossover, replacement mutation, and rank-based selection, with fitness scores assessing variables encoded into multi-dimensional vectors updated across iterations.

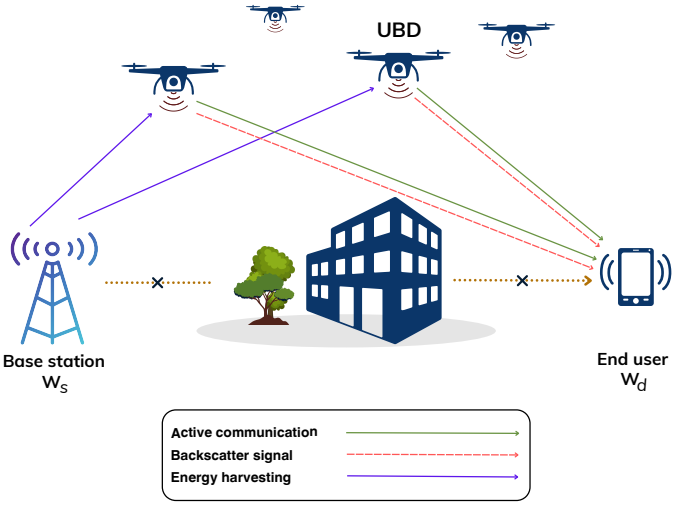

Fig. 1. The considered system model with multiple-UAV trajectory of UAVs

The paper is as follows. Section II outlines the system model and problem formulation. Section III details the iterative algorithm for solving the linear EH model in a 3D UAV-enabled BackCom network. Section IV presents the GA-based optimization method. Section V discusses numerical results, and Section VI concludes the paper.

II. Communication System and Signal Models

In this research, we investigate a network system consisting of multiple UAVs operating in 3D space, enhanced by cache technology and backscatter circuitry. The communication network model is described as in Fig. 1. Assume that the base station is located at the source S and the end user is positioned at the destination D. The coordinates of S and D are fixed at $\mathbf{W}_s$ and $\mathbf{W}_d$ respectively. We focus on a scenario where data is transmitted from a source to a destination in a non-line-of-sight environment or under severe fading conditions. It is assumed that user are successfully served by the data source.

A. Propagation Channel Model

UAVs, recognized as advanced technology, play a vital role in ensuring reliable data transmission within modern networks, facilitating seamless communication. This study focuses on the communication links between the source and UBDs, and between UBDs and the destination. To make the optimization problem solvable and provide flexibility for adjustments as the user at D changes location, T is defined as the total duration for a UBD to travel from its initial to final location and serve the destination. The time window T is divided into N slots, each lasting $\delta t = T/N$. The m-th UBD's location during the n-th slot is expressed as $\mathbf{q}_n^m$, $\forall\ n \in \mathcal{N} \triangleq \{0, ..., N\}$, $m \in \mathcal{M} \triangleq \{1, ..., M\}$. Representing the maximum UBD speed as $V_{\max}$, the positions of the m-th UBD between consecutive slots $(n+1)$ and n, $\forall\ n \in \mathcal{N}$, must satisfy the following constraints:

$$\Delta_n^m \triangleq \left\|\mathbf{q}_{n+1}^m - \mathbf{q}_n^m\right\| \leq V_{\max}\delta_t,\ \forall n \in \mathcal{N}, \forall m \in \mathcal{M}, \quad (1)$$

$$\mathbf{q}_0^m = \mathbf{q}_I^m,\ \mathbf{q}_N^m = \mathbf{q}_F^m. \quad (2)$$

Here, $\mathbf{q}_I^m$ represents the initial location of the m-th UB, while $\mathbf{q}_F^m$ represents its final location. Constraint (1) requires that the distance covered by the UBD between two successive time slots, specifically from time interval n to $n+1$, does not exceed the maximum permissible flight distance within the given time duration δ_t. Additionally, constraint (2) imposes that the UBD's trajectory must begin and conclude at the fixed coordinates of points $\mathbf{q}_I^m$ and $\mathbf{q}_F^m$, respectively. The term $\left\|\mathbf{q}_{n+1}^m - \mathbf{q}_n^m\right\|$ denotes the Euclidean norm of the vector $\left[\mathbf{q}_{n+1}^m - \mathbf{q}_n^m\right]$. To maintain consistency in notation, we will refer to the source, destination, and UBD as *s*, *d*, and *u*, respectively. Thus, $\forall\ n \in \mathcal{N}$, the distances between the source and the m-th UBD (for the incoming wave) and between the m-th UBD and the destination (for the backscattered wave) during the *n*-th time slot can be expressed as

$$d_{su}^{nm} = \left\|\mathbf{q}_n^m - \mathbf{W}_s\right\|, d_{du}^{nm} = \left\|\mathbf{q}_n^m - \mathbf{W}_d\right\|. \quad (3)$$

In our investigation, a comprehensive fading channel model is considered, incorporating both line-of-sight (LoS) and non-line-of-sight (NLoS) components. This model reflects the deployment of UAVs across diverse radio environments, including rural, urban, and suburban areas. Additionally, we meticulously examine the impact of large-scale and small-scale fading effects to effectively characterize the random fluctuations inherent in the environment [28]. By analyzing the interaction between these factors, we aim to gain a deeper understanding of the complex dynamics and inherent uncertainties governing the fading characteristics of the channel. The channel coefficient h_{iu}^{nm} for m-th UB, $\forall\ i \in \{s, d\}$, during the *n*-th time slot, is given by the formula:

$$h_{iu}^{nm} = \sqrt{\psi_{iu}^{nm}}\widetilde{h}_{iu}^{nm} = \sqrt{\omega_0 (d_{iu}^{nm})^{-\alpha}}\widetilde{h}_{iu}^{nm}, \quad (4)$$

where ψ_{iu}^{nm} and $\widetilde{h}_{iu}^{nm}$ represent the symbols for large-scale fading and small-scale fading, respectively, in time slot n. Here, w_0 is the reference channel gain with d_{iu}^{nm} equal to one meter, and α represents the path loss exponent. The small-scale fading component $\widetilde{h}_{iu}^{nm}$ can be expressed as:

$$\widetilde{h}_{iu}^{nm} = \sqrt{\frac{K}{1+K}}\bar{h}_{iu}^{nm} + \sqrt{\frac{1}{1+K}}\hat{h}_{iu}^{nm}, \quad (5)$$

where $\bar{h}_{iu}^{nm}$ represents the deterministic LoS component, and $\hat{h}_{iu}^{nm}$ denotes the NLoS component. The Rician factor K influences the complex dynamics of the fading process.

B. Caching Model and Limited Transmit Power Budget

In order to minimize latency, increase data speed, and improve transmission efficiency, each UBD is provisioned with additional cache memory. This added memory facilitates the pre-loading of part of the data intended for transmission, thereby optimizing the overall data transfer process. In more detail, each UBD retains a fraction of the data source within its cache. Let σ represent the proportion of the data source stored by the caching model, where $0 \leq \sigma \leq 1$, and let M denote the number of UBDs. When the destination requests a data source, a segment σ of this file is already available in the storage of each UBD. Utilizing the caching mechanism, the source transmits only a portion of the data source to the destination via the UBDs, with the transmitted amount being proportional to $(1 - M\sigma)$. It is important to note that this caching model represents a lower bound for scenarios where the UAVs have prior knowledge of content popularity.

To optimize throughput at the destination and allow for flexible energy allocation in each time slot, we impose a constraint on the total transmission energy, ensuring it does not become excessively large. This constraint is expressed as follows:

$$0 \leq P_s^{nm} + P_u^{nm} \leq P_{\max}, \quad (6)$$

where $P_{\max}$ is the maximum allowable total transmit power, P_s^m is defined as the transmit power of the source to the UBD m and P_u^m is the transmit power of UBD m. At time slot n, these are denoted as P_u^{nm} and P_s^{nm}, respectively.

C. Energy Harvesting and Energy Consumption

Given the constrained power budget, it becomes imperative to consider energy harvesting to extend the operational lifespan of UBDs. To achieve this objective, a dynamic time-splitting mechanism is devised, which partitions each time slot into two phases for UBD communication. It is essential to emphasize that the duration of each phase is adaptable and subject to variation across different time slots. For the m-th UB, a portion τ_n^m of each time slot is designated for backscattering signal transmission, while the remainder $(1-\tau_n^m)$ is used for energy harvesting. Specifically, during a time slot of length δ_t, the UBD spends $\tau_n^m\delta_t$ for transmission of backscattering signals and $(1-\tau_n^m)\delta_t$ for energy harvesting. The energy harvested by the UB, denoted as E_h^{nm}, is calculated as follows [29]:

$$E_h^{nm} \triangleq \mu\left(1-\tau_n^m\right)\delta_t P_{WPT}\mathbb{E}[|h_{su}^{nm}|^2], \quad (7)$$

where P_{WPT} represents the transmit power of the source used during the energy harvesting phase, which lasts for $(1-\tau_n^m)$ δ_t in the n-th time slot. The energy harvesting efficiency, denoted by μ, corresponds to the linear model of electromagnetic energy harvesters. The parameter τ_n^m signifies dynamic time-division duplexing within each time slot. For instance, when τ_n^m = 1, the entire slot is allocated for backscattering signals to the destination. Conversely, when τ_n^m = 0, the entire slot is dedicated to energy harvesting. The expectation of the channel coefficient is given as:

$$\mathbb{E}[|h_{su}^{nm}|^2] = \omega_0/(d_{su}^{nm})^{\alpha}. \quad (8)$$

The classification of energy consumption for UBDs involves three main components: energy used for backscattering, energy expended on propulsion, and energy required for active communication with the destination. Specifically, the energy consumed by the m-th UBD for propulsion during the n-th time slot, denoted as E_{fly}^{nm}, is calculated using the model presented in [30] as:

$$E_{fly}^{nm}(\mathbf{q}) = P_0(\delta_t + \frac{k_1}{\delta_t}(\Delta_n^m)^2) + P_1\sqrt{\sqrt{\delta_t^4 + k_2^2(\Delta_n^m)^4} - k_2(\Delta_n^m)^2} + \frac{k_3(\Delta_n^m)^3}{\delta_t^2}, \quad (9)$$

TABLE I
EXPERIMENTAL DATA

Parameters	Values
ρ	1.225 kg/m^3
I	0.1
A	0.8 m^2
δ	0.1
W	0.5 N
Ω	100 rad/s
R	0.08 m
s	0.05

where $P_0 = \frac{\delta}{8}\rho s A \Omega^3 R^3$, $P_1 = (1+I)\frac{W^{3/2}}{\sqrt{2\rho A}}$, $k_1 = \frac{3}{\Omega^2 R^2}$, $k_2 = \frac{1}{2v_0^2}$, $k_3 = 0.5 d_0 \rho s A$. The model incorporates the profile drag coefficient δ, air density ρ [kg/m^3], rotor solidity s, rotor disc area A [m^2], blade angular velocity Ω [rad/s], rotor radius R [m], an incremental adaptation value I (set to 0.1) concerning the induced power, and UAV weight W [N] with specific values shown in Table I. During the n-th time slot, the model in (9) determines the energy consumed by the UAV's backscatter equipment, represented as $\tau_n^m \delta_t P_b$, where P_b denotes the UAV's hardware power consumption during the backscatter phase [29]. An energy constraint for the UBD can be established, incorporating all the parameters mentioned:

$$\sum\nolimits_{i=1}^{n} \left(E_{fly}^{nm}(\mathbf{q}) \ + \ \tau_n^m \delta_t \ (P_b \ + \ P_u^m)\right) \leq \sum\nolimits_{i=1}^{n} E_h^{nm}. \tag{10}$$

This suggests that the total energy harvested by the UBD by time slot n should exceed its cumulative energy consumption. By combining (7) to (10), a closed-form expression for the constraint in (10) can be derived:

$$\sum\nolimits_{i=1}^{n} \left(E_{fly}^{nm}(\mathbf{q}) + \tau_n^m \delta_t (P_b + P_u^m)\right) \leq \sum\nolimits_{i=1}^{n} \frac{\mu \left(1-\tau_n^m\right) \delta_t \omega_0 P_{WPT}}{(d_{su}^{nm})^{\alpha}}. \tag{11}$$

D. Signal Model and Shannon Capacity

Given their role as backscattering nodes, UBD networks effectively disperse incoming waves from the source to the destination. To reduce interference between uplink (UL) and downlink (DL) transmissions, a time-division duplexing (TDD) system is employed, as extensively discussed in [27]. Each time slot is divided into two segments using the dynamic time splitting method: the intervals $\left(1-\tau_n^m\right)\delta_t$ and $\tau_n^m \delta_t$ are respectively allocated for uplink data transmission from the source to the UB, and downlink data transmission from the UBD to the destination. The dynamic time splitting ratio for the n-th time slot adheres to the constraint $0 \leq \tau_n^m \leq 1$. Denoting v_s^{nm} as the complex data symbol transmitted by the source to the m-th UBD with unit power ($\mathbb{E}\left[|v_s^{nm}|^2\right] = 1$) during the n-th time slot, the received signal at m-th UBD can be expressed as:

$$g_u^{nm} = \sqrt{P_s^{nm}} h_{su}^{nm} v_s^{nm} + n_u, \tag{12}$$

where $n_u \sim \mathcal{CN}\left(0, \sigma_u^2\right)$ represents the additive white Gaussian noise (AWGN) at the UB. Furthermore, the signal v_u^{nm}, resulting from the backscattering by UBD m during the n-th time slot, is given by [31]:

$$v_u^{nm} = \sqrt{\eta_u^n P_s^{nm}} h_{su}^{nm} v_s^{nm}, \tag{13}$$

whereas η_u^n, ranging from 0 to 1, denotes the backscatter coefficient for time slot n. Furthermore, the disregarded factors in equation (13), such as supplementary noise and signal processing latency, are crucial and well-documented in prior studies [29], [31], [32]. With the active link provided by the UBD m, the formulation of the signal received at the destination unfolds as follows:

$$g_d^{nm} = h_{ud}^{nm} v_u^{nm} + \sqrt{P_u^{nm}} h_{ud}^{nm} v_s^{nm} + n_d. \tag{14}$$

The term n_d, representing the additive white Gaussian noise (AWGN) at the destination, follows a distribution $n_d \sim \mathcal{CN}\left(0, \sigma_u^2\right)$. The received signal at the destination due to backscattering and active data transmission from source S and the m-th UBD during time slot n is denoted by $\sqrt{P_s^{nm}} h_{ud}^n v_s^{nm}$ and $\sqrt{P_u^{nm}} h_{ud}^n v_s^{nm}$, respectively. It is important to note that the noise power from backscattering, denoted as $\sqrt{\eta_u^n n_u}$ in equation (14), is much lower than the baseband noise power [33] and is thus considered negligible in the equation's formulation. The overall received signal at the destination, integrating the contributions from (13) and (14), is

$$g_d^{nm} = \sqrt{\eta_u^n P_s^{nm}} h_{ud}^{nm} h_{su}^{nm} v_s^{nm} + \lceil \sigma \rceil \sqrt{P_u^{nm}} h_{ud}^{nm} v_c^{nm} + n_d, \tag{15}$$

where v_c^{nm} represents the transmitted data symbol cached within the UBD m, with an expected power of $\mathbb{E}\left[|v_c^{nm}|^2\right] = 1$. $\lceil \sigma \rceil$ denotes the ceiling function of σ. The term $\sqrt{P_u} h_{ud}^n v_c^n$ indicates that if a σ fraction of the requested file is cached within the UBD's storage, the UBD can then transmit the cached signal to the destination. Consequently, the signal-to-noise ratio (SNR) at the destination can be expressed as follows:

$$\mathrm{SNR}_d^{nm} = \frac{\eta_u^n P_s^{nm} |h_{ud}^{nm}|^2 |h_{su}^{nm}|^2 + P_u^{nm} \lceil \sigma \rceil |h_{ud}^{nm}|^2}{\sigma_d^2}. \tag{16}$$

Here, the variance of noise power at the destination, n_d, is indicated by σ_d^2 in the equation. In the n-th time slot, the data throughput, measured in bps, at the UBD m and the destination can be respectively computed as follows:

$$R_u^{nm} = B \log_2 \left(1 + \mathrm{SNR}_u^{nm}\right), \tag{17}$$

$$R_d^{nm} = B \log_2 \left(1 + \mathrm{SNR}_d^{nm}\right), \tag{18}$$

where B (Hz) represents the system bandwidth and $\mathrm{SNR}_u^{nm} = P_s^{nm} |h_{su}^{nm}|^2 / \sigma_u^2$. Notably, the instantaneous Channel State Information (CSI), including h_{su}^{nm} and h_{ud}^{nm}, is characterized as a random variable. Consequently, the instantaneous data throughput also exhibits the characteristics of a random variable. In light of this, we consider the approximated received data throughputs for the UBD and the destination, which can be formulated as follows:

$$\bar{R}_u^{nm} = B\mathbb{E}\left[\log_2 \left(1 + \mathrm{SNR}_u^{nm}\right)\right], \tag{19}$$

$$\bar{R}_d^{nm} = B\mathbb{E}\left[\log_2 \left(1 + \mathrm{SNR}_d^{nm}\right)\right]. \tag{20}$$

Deriving a closed-form expression for $\bar{R}_u^{nm}$ and $\bar{R}_d^{nm}$ is a challenging task. Consequently, Lemma 1 that follows provides the expressions for $\bar{R}_u^{nm}$ and $\bar{R}_u^{nm}$ through approximation functions.

Lemma 1. *Approximations for $\bar{R}_u^{nm}$ and $\bar{R}_d^{nm}$ can be formulated using closed-form expressions as follows:*

$$\bar{R}_u^{nm} = B\log_2\left(1+\frac{e^{-E}w_0P_s^{nm}}{(d_{su}^{nm})^{\alpha}\sigma_u^2}\right), \tag{21}$$

$$\bar{R}_d^{nm} = B\log_2\left(1+\frac{\theta(\eta_u^n w_0 P_s^{nm} + \bar{P}_u^{nm}(d_{su}^{nm})^{\alpha})}{\varrho}\right), \tag{22}$$

where $\theta \triangleq \frac{e^{-E}\omega_0}{\sigma_d^2}$, $\bar{P}_u^{nm} \triangleq P_u^{nm}\lceil\sigma\rceil$, $\varrho \triangleq (d_{su}^{nm})^{\alpha}(d_{du}^{nm})^{\alpha}$.

Proof. We consider a function $f(x) = \mathbb{E}\left[\log_2(1+x)\right], x>0$. Consequently, $f(x) = \mathbb{E}\left[\log_2(1+e^{\ln x})\right], x>0$. By applying Jensen's inequality to the convex function $\log_2(1+e^{\ln x})$ with respect to $\ln x$ variable, we get:

$$f(x) \geq \log_2(1+e^{\mathbb{E}[\ln x]}), \tag{23}$$

Denoting $x \triangleq P_s^{nm}|h_{su}^{nm}|^2/\sigma_u^2$, x is an independent random variable following an exponential distribution with rate parameter $\lambda_f = \mathbb{E}[x]^{-1} > 0$. Hence, $\lambda_f = (P_s^{nm}\omega_0(d_{su}^{nm})^{-\alpha}/\sigma_u^2)^{-1}$. Using [[34], 4.331.1], we have:

$$\begin{aligned}\mathbb{E}[\ln x] &= \int_0^{+\infty}\lambda_f e^{-\lambda_f x}\ln x dx = -(\ln\lambda_f + E)\\ &= \ln(P_s^{nm}\omega_0(d_{su}^{nm})^{-\alpha}/\sigma_u^2) - E,\end{aligned} \tag{24}$$

where $E = 0.5772156649$ [[34], 4.331.1] is the Euler-Mascheroni constant. Equation expression (21) can be obtained by replacing (24) with (23).

To prove (22), we consider a function $w(x,y) = \mathbb{E}\left[\log_2(1+xy)\right], x>0, y>0$ with x, y are independent random variables. Applying Jensen's inequality to the concave function $\log_2(1+xy)$ with respect to y variable, we get:

$$w(x,y) \leq \log_2(1+x\mathbb{E}[y]) \triangleq \tilde{w}(x,y). \tag{25}$$

Consequently, $\tilde{w}(x,y) = \log_2(1+e^{\ln x}\mathbb{E}[y])$. Using Jensen's inequality for the convex function $\tilde{w}(x,y)$ with respect to $\ln x$ variable, we get:

$$\tilde{w}(x,y) \geq \log_2(1+e^{\ln\mathbb{E}[x]}\mathbb{E}[y]) \triangleq \hat{w}(x,y). \tag{26}$$

It is observed that $\tilde{w}(x,y)$ can effectively approximate $w(x,y)$, although it does not serve as a definitive lower or upper bound. By applying [[34], 4.331.1] and using the notations $x = |h_{ud}^{nm}|^2$, $y = (\eta_u^n P_s^{nm}|h_{su}^{nm}|^2 + P_u^{nm}\lceil\sigma\rceil)/\sigma_d^2$, we then obtain the following expression:

$$\begin{aligned}\mathbb{E}[\ln x] &= \int_0^{+\infty}\lambda_g e^{-\lambda_g x}\ln x dx = -(\ln\lambda_g + E)\\ &= \ln(\frac{\omega_0}{(d_{su}^{nm})^{\alpha}}) - E,\end{aligned} \tag{27}$$

$$\mathbb{E}[y] = \frac{\eta_u^n P_s^{nm}\omega_0(d_{su}^{nm})^{-\alpha} + \bar{P}_u^{nm}}{\sigma_d^2} \tag{28}$$

where $\lambda_g = \mathbb{E}[x]^{-1} = (\omega_0/(d_{su}^{nm})^{\alpha})^{-1}$. The expression in equation (22) can be obtained by substituting (27) and (28) into (26). Consequently, Lemma 1 is conclusively proved. □

E. Problem Formulation

The objective of this section is to develop a mathematical formulation aimed at maximizing the total data transmission from each UBD to the destination. This is achieved by jointly optimizing the DTS ratio, UBD trajectory and total transmit power under a linear EH mode. To formalize this optimization problem, we define $\mathbf{q} \triangleq \{\mathbf{q}_n^m; n\in\mathcal{N}, m\in\mathcal{M}\}$, $\boldsymbol{\tau} \triangleq \{\tau_n; n\in\mathcal{N}\}$, and $\mathbf{P} \triangleq \{P_u^n, P_s^n; n\in\mathcal{N}, m\in\mathcal{M}\}$. The problem is mathematically formulated as follows:

$$\mathcal{P}_1: \underset{\mathbf{q},\boldsymbol{\tau},\mathbf{P}}{\text{maximize}} \sum\nolimits_{m\in\mathcal{M}}\sum\nolimits_{n\in\mathcal{N}}\tau_n^m\delta_t\bar{R}_d^{nm}, \tag{29a}$$

$$\text{s.t.} \sum_{n\in N}\tau_n^m\delta_t\bar{R}_u^{nm} + \sigma S \geq \sum_{n\in N}\tau_n^m\delta_t\bar{R}_d^{nm}, \forall m\in\mathcal{M}, \tag{29b}$$

$$\sum\nolimits_{n\in N}\tau_n^m\delta_t\bar{R}_d^{nm} \geq S, \forall m\in\mathcal{M}, \tag{29c}$$

$$\begin{aligned}&\sum\nolimits_{i=1}^{n}\left(E_{fly}^{nm}(\mathbf{q}) + \tau_n^m\delta_t\left(P_b + P_u^{nm}\right)\right)\\ &\qquad\leq \sum\nolimits_{i=1}^{n}\frac{\mu(1-\tau_n^m)\delta_t w_0 P_{WPT}}{(d_{su}^{nm})^{\alpha}}, \forall m\in\mathcal{M},\end{aligned} \tag{29d}$$

$$0 \leq P_u^{nm} + P_s^{nm} \leq P_{\max}, \forall m\in\mathcal{M}, \forall n\in\mathcal{N}, \tag{29e}$$

$$\left\|\mathbf{q}_{n+1}^m - \mathbf{q}_n^m\right\| \leq \delta_d = V_{\max}\delta_t, \forall m\in\mathcal{M}, \forall n\in\mathcal{N}, \tag{29f}$$

$$\mathbf{q}_0^m = \mathbf{q}_I^m,\ \mathbf{q}_N^m = \mathbf{q}_F^m, \forall m\in\mathcal{M}, \tag{29g}$$

$$0 \leq \tau_n^m \leq 1, \forall n\in N, \forall m\in\mathcal{M}. \tag{29h}$$

Here, S represents the data demanded by the destination in bits. Constraint (29b) ensures that the data transmitted from the UBD must exceed the data received by the destination. Constraint (29c) stipulates that the total data transmitted on the DL from a UBD must meet or exceed the destination's data requirements, ensuring adherence to technical requirements and user demands. Constraint (29d) mandates that the energy consumed by the UBD for flight, backscatter, and communication should not exceed its harvested energy. Constraint (29e) specifies that the maximum allowable power value should not be exceeded by the transmission energy of both the source and the UBD during the transmission.

Problem $\mathcal{P}_1$ is a challenging non-convex optimization problem because its objective function and constraints (29b), (29c), (29d) are non-convex, making it hard to solve. Finding a direct solution for $\mathcal{P}_1$ is problematic due to this non-convexity.

III. BCD-BASED SOLUTION

To effectively tackle the complexity of Problem $\mathcal{P}_1$, we decompose it into three manageable sub-problems. First, we focus on optimizing the DTS ratio with fixed trajectory and initial power transmission values. Subsequently, we optimize the UBD trajectory, maintaining the DTS ratio fixed from the previous step and using a same initial power transmission value. Finally, we optimize the total transmit power by considering the DTS ratio and trajectory obtained in the preceding steps. Using the block coordinate descent (BCD) technique [35], we employ an efficient iterative algorithm based on KKT conditions, in which we iteratively optimize these three subproblems until the algorithm converges, with the optimization threshold $\epsilon \geq 0$ greater than 0.

A. Joint Path Planning & Dynamic Time Splitting Optimization

Given a trajectory $\mathbf{q}$ and initial power transmission values $\mathbf{P}$ for each UBD. The following optimization problem is formulated to obtain the DTS ratio $\boldsymbol{\tau}$ of the m-th UBD:

$$\mathcal{P}_1^{\boldsymbol{\tau}}: \underset{\boldsymbol{\tau}}{\text{maximize}} \sum\nolimits_{m\in\mathcal{M}}\sum\nolimits_{n\in\mathcal{N}} \tau_n^m \delta_t \bar{R}_d^{nm} \tag{30a}$$

$$\text{s.t.} \sum\nolimits_{n\in N} \tau_n^m \delta_t \bar{R}_u^{nm} + \sigma S \geq \sum\nolimits_{n\in N} \tau_n^m \delta_t \bar{R}_d^{nm}, \forall m \in \mathcal{M}, \tag{30b}$$

$$\sum\nolimits_{n\in N} \tau_n^m \delta_t \bar{R}_d^{nm} \geq S, \forall m \in \mathcal{M}, \tag{30c}$$

$$\sum\nolimits_{i=1}^{n} \left(E_{fly}^{nm}(\mathbf{q}) + \tau_n^m \delta_t \left(P_b + P_u^{nm}\right)\right) \leq \sum\nolimits_{i=1}^{n} \frac{\mu(1-\tau_n^m)\delta_t w_0 P_{WPT}}{(d_{su}^{nm})^{\alpha}}, \forall m \in \mathcal{M}, \tag{30d}$$

$$0 \leq \tau_n^m \leq 1, n \in N, \forall m \in \mathcal{M}. \tag{30e}$$

It can be readily confirmed that the Slater's condition is satisfied by $\mathcal{P}_1^{\boldsymbol{\tau}}$, making the KKT conditions sufficient for optimality because problem $\mathcal{P}_1^{\boldsymbol{\tau}}$ is evidently a linear optimization problem and therefore it is convex [36]. The Lagrangian function corresponding to problem $\mathcal{P}_1^{\boldsymbol{\tau}}$ is expressed as follows:

$$\mathcal{L}\left(\boldsymbol{\tau}, \lambda_1, \lambda_2, \lambda_3, \lambda_4\right) \triangleq F(\boldsymbol{\tau}) + \lambda_1 G(\boldsymbol{\tau}) + \lambda_2 H(\boldsymbol{\tau}) + \lambda_3 I(\boldsymbol{\tau}) + \lambda_4 J(\boldsymbol{\tau}), \tag{31}$$

where the following definitions hold

$$F(\boldsymbol{\tau}) \triangleq \sum\nolimits_{n\in\mathcal{N}} \tau_n^m \delta_t \bar{R}_d^{nm}, \tag{32}$$

$$G(\boldsymbol{\tau}) \triangleq \sum\nolimits_{n\in N} \tau_n^m \delta_t \bar{R}_u^{nm} + \sigma S - \sum\nolimits_{n\in N} \tau_n^m \delta_t \bar{R}_d^{nm} \geq 0, \tag{33}$$

$$H(\boldsymbol{\tau}) \triangleq \sum\nolimits_{n\in N} \tau_n^m \delta_t \bar{R}_d^{nm} - S \geq 0, \tag{34}$$

$$I(\boldsymbol{\tau}) \triangleq \sum\nolimits_{i=1}^{n} \frac{\mu(1-\tau_n^m)\delta_t w_0 P_{WPT}}{(d_{su}^{nm})^{\alpha}} - \sum\nolimits_{i=1}^{n} \left(E_{fly}^{nm}(\mathbf{q}) + \tau_n^m \delta_t \left(P_b + P_u^{nm}\right)\right) \geq 0, \tag{35}$$

$$J(\boldsymbol{\tau}) \triangleq 1 - \tau_n \geq 0, \tag{36}$$

where λ_1, λ_2, λ_3, λ_4 are Lagrangian dual variables. Here, (33), (34), (35), and (36) are the primal feasibility conditions. Subsequently, the following expressions represent the complementary slackness conditions:

$$\lambda_1 G\left(\boldsymbol{\tau}\right) = 0, \lambda_2 H\left(\boldsymbol{\tau}\right) = 0, \lambda_3 I\left(\boldsymbol{\tau}\right) = 0, \lambda_4 J\left(\boldsymbol{\tau}\right) = 0, \tag{37}$$

with the given stationarity condition:

$$\frac{\partial L(\tau, \lambda_1, \lambda_2, \lambda_3, \lambda_4)}{\partial \tau} = \sum\nolimits_{n\in\mathcal{N}} \delta_t \bar{R}_d^{nm} + \lambda_1 \left(\sum\nolimits_{n\in N} \delta_t \bar{R}_u^{nm} - \sum\nolimits_{n\in N} \delta_t \bar{R}_d^{nm}\right) + \lambda_2 \sum\nolimits_{n\in\mathcal{N}} \delta_t \bar{R}_d^{nm} - \lambda_3 \left(\sum\nolimits_{n\in N} X_1 + \sum\nolimits_{n\in N} \delta_t \left(P_b + P_u^{nm}\right)\right) - \lambda_4 = 0. \tag{38}$$

where $X_1 \triangleq (\mu\delta_t\omega_0 P_{WPT})/(d_{su}^{nm})^{\alpha}$. For an optimal solution to be feasible, the dual feasibility conditions should be satisfied with $\lambda_1, \lambda_2, \lambda_3, \lambda_4 \geq 0$. The solution that maximizes the objective function in $\mathcal{P}_1^{\boldsymbol{\tau}}$ is selected to achieve this optimal outcome. In the following theorem, two possible solutions for the optimal value of $\boldsymbol{\tau}$ are postulated.

Theorem 1. *The optimal value for problem $\mathcal{P}_1^{\boldsymbol{\tau}}$, denoted as $\{\tau_n^{m*}\}$, can be represented as follows:*

$$\tau_n^{m*} = \frac{\sigma S}{N\delta_t\left(\bar{R}_d^{nm} - \bar{R}_u^{nm}\right)}, iff\ \bar{R}_d^{nm} > \bar{R}_u^{nm}, \quad \forall n \in \mathcal{N}, \forall m \in \mathcal{M}, \tag{39a}$$

$$\tau_n^{m*} = \frac{X_1 - E_{fly}^{nm}\left(\mathbf{q}\right)}{X_1 + \delta_t\left(P_b + P_u^{nm}\right)}. \tag{39b}$$

Proof. If $J(\boldsymbol{\tau}) = 0$, it implies that $\tau_n^m = 1$, which is not a feasible solution. Therefore, we deduce that $\lambda_4 = 0$. To find a feasible solution, we examine all possible cases as follows:

Case 1: $\lambda_1 = 0$, $\lambda_2 = 0$, $\lambda_3 = 0$.

According to equation (38), $\sum_{n\in\mathcal{N}} \delta_t \bar{R}_d^{nm} = 0$, which is not a reasonable outcome. Therefore, this case is not possible.

Case 2: $\lambda_1 = 0$, $H(\boldsymbol{\tau}) = 0$, $I(\tau) = 0$.

From $H(\boldsymbol{\tau}) = 0$, it follows that $\tau_n^m = \frac{S}{N\delta_t \bar{R}_d^{nm}}$. Similarly, from $I(\boldsymbol{\tau}) = 0$, we find $\tau_n^m = \frac{X_1 - E_{fly}^{nm}(\mathbf{q})}{X_1 + \delta_t(P_b + P_u^{nm})}$. This results in two different optimal values for τ, which is contradictory. Therefore, this case is not possible.

Case 3: $G(\boldsymbol{\tau}) = 0$, $\lambda_2 = 0$, $I(\boldsymbol{\tau}) = 0$.

Case 4: $G(\boldsymbol{\tau}) = 0$, $H(\boldsymbol{\tau}) = 0$, $\lambda_3 = 0$.

As in case 2, case 3 and case 4 also get two different values for τ. Therefore, these cases are not possible.

Case 5: $G(\boldsymbol{\tau}) = 0$, $H(\boldsymbol{\tau}) = 0$, $I(\boldsymbol{\tau}) = 0$.

In this case, we get up to three different τ values, which is absurd. As a result, this case is not possible.

Case 6: $G(\boldsymbol{\tau}) = 0$, $\lambda_2 = 0$, $\lambda_3 = 0$.

From equation (38), we find $\lambda_1 = \frac{\sum_{n\in\mathcal{N}} \delta_t \bar{R}_d^{nm}}{\sum_{n\in N} \delta_t \bar{R}_d^{nm} - \sum_{n\in N} \delta_t \bar{R}_u^{nm}}$. If $\bar{R}_u^{nm} = \bar{R}_d^{nm}$, then $\lambda_1 = +\infty$. If $\bar{R}_u^{nm} > \bar{R}_d^{nm}$, then $\lambda_1 < 0$. Both scenarios are unreasonable. If $\bar{R}_u^{nm} < \bar{R}_d^{nm}$, then $\lambda_1 > 1$. Additionally, given $G(\boldsymbol{\tau}) = 0$, we have

$$\tau_n^m = \frac{\sigma S}{N\delta_t(\bar{R}_d^{nm} - \bar{R}_u^{nm})}. \tag{40}$$

According to equation (39), the optimal solution $\{\tau_n^{m*}\}$ can be determined when $\bar{R}_u^{nm} < \bar{R}_d^{nm}, \forall n \in \mathcal{N}, \forall m \in \mathcal{M}$.

Case 7: $\lambda_1 = 0$, $H(\boldsymbol{\tau}) = 0$, $\lambda_3 = 0$.

From equation (38), $\lambda_2 = -1$, which is not a reasonable outcome. Therefore, this case is not possible.

Case 8: $\lambda_1 = 0$, $\lambda_2 = 0$, $I(\boldsymbol{\tau}) = 0$.

From equation (38), we have:

$$\lambda_3 = \frac{\sum_{n\in\mathcal{N}} \delta_t \bar{R}_d^{nm}}{\sum_{n\in N} X_1 + \sum_{n\in N} \delta_t\left(P_b + P_u^{nm}\right)} \geq 0. \tag{41}$$

Additionally, given $I(\boldsymbol{\tau}) = 0$, we have:

$$\tau_n^m = \frac{X_1 - E_{fly}^{nm}\left(\mathbf{q}\right)}{X_1 + \delta_t\left(P_b + P_u^{nm}\right)}. \tag{42}$$

We can derive (39) by combining (40), (42), and constraint (30a), completing the proof of Theorem 1. □

In which $E_{fly}^{nm}(\mathbf{q})$, $\bar{R}_u^{nm}$, $\bar{R}_d^{nm}$, X_1 are updated each time the loop calculates τ_n^m. To attain the optimal result, the solution that yields the maximum value of the objective function in $\mathcal{P}_1^{\boldsymbol{\tau}}$ is selected. The feasibility set, i.e., $0 \leq \tau_n^m \leq 1$, must ensure that the optimal value of $\{\tau_n^{m*}\}$ obtained from (39a) and (39b) is within its bounds.

B. Proceed With Trajectory Optimization

For a given $\boldsymbol{\tau}$ and $\mathbf{P}$, UBDs's trajectories $\mathbf{q}$ can be determined by solving the following problems:

$$\mathcal{P}_1^{\mathbf{q}}: \underset{\mathbf{q}}{\text{maximize}} \sum\nolimits_{m\in\mathcal{M}} \sum\nolimits_{n\in\mathcal{N}} \tau_n^m \delta_t \bar{R}_d^{nm} \tag{43a}$$

$$\text{s.t.} \sum\nolimits_{n\in N} \tau_n^m \delta_t \bar{R}_u^{nm} + \sigma S \geq \sum\nolimits_{n\in N} \tau_n^m \delta_t \bar{R}_d^{nm}, \forall m \in \mathcal{M}, \tag{43b}$$

$$\sum\nolimits_{n\in N} \tau_n^m \delta_t \bar{R}_d^{nm} \geq S, \forall m \in \mathcal{M}, \tag{43c}$$

$$\sum\nolimits_{i=1}^{n} \left(E_{fly}^{nm}(\mathbf{q}) + \tau_n^m \delta_t \left(P_b + P_u^{nm}\right)\right) \leq \sum\nolimits_{i=1}^{n} \frac{\mu(1-\tau_n^m)\delta_t w_0 P_{WPT}}{(d_{su}^{nm})^{\alpha}}, \forall m \in \mathcal{M}, \tag{43d}$$

$$\left\|\mathbf{q}_{n+1}^m - \mathbf{q}_n^m\right\| \leq \delta_d = V_{\max}\delta_t, \forall m \in \mathcal{M}, \forall n \in \mathcal{N}, \tag{43e}$$

$$\mathbf{q}_0^m = \mathbf{q}_I^m,\ \mathbf{q}_N^m = \mathbf{q}_F^m, \forall m \in \mathcal{M}. \tag{43f}$$

The non-convexity of problem $\mathcal{P}_1^{\mathbf{q}}$ complicates solving it with standard optimization methods. To address this, the SCA technique is utilized. Introducing slack variables a_m^n and b_m^n, where $\|\mathbf{q}_n^m - \mathbf{W}_s\|^{\alpha} \leq a_m^n$ and $\|\mathbf{q}_n^m - \mathbf{W}_d\|^{\alpha} \leq b_m^n$, enhances tractability. These variables, denoted as $\mathbf{z} \triangleq \{a_m^n, b_m^n, n \in \mathcal{N}\}$, allow problem $\mathcal{P}_1^{\mathbf{q}}$ to be rewritten as follows:

$$\mathcal{P}_{1.1}^{\mathbf{q}}:$$

$$\underset{\mathbf{q},\mathbf{z}}{\text{maximize}}\ B \sum_{m\in\mathcal{M}} \sum_{n\in\mathcal{N}} \tau_n^m \delta_t \log_2\left(1 + \frac{\theta(\Theta + \bar{P}_u^{nm} a_m^n)}{a_m^n b_m^n}\right) \tag{44a}$$

$$\text{s.t.} \quad \|\mathbf{q}_n^m - \mathbf{W}_s\|^{\alpha} \leq a_m^n, \forall m \in \mathcal{M}, \forall n \in \mathcal{N}, \tag{44b}$$

$$\|\mathbf{q}_n^m - \mathbf{W}_d\|^{\alpha} \leq b_m^n, \forall m \in \mathcal{M}, \forall n \in \mathcal{N}, \tag{44c}$$

$$B \sum\nolimits_{n\in N} \tau_n^m \delta_t \log_2\left(1 + \frac{e^{-E} w_0 P_s^{nm}}{a_m^n \sigma_u^2}\right) + \sigma S \geq B \sum\nolimits_{n\in N} \tau_n^m \delta_t \log_2\left(1 + \frac{\theta(\eta_u^n w_0 P_s^{nm} + \bar{P}_u^{nm} a_m^n)}{a_m^n b_m^n}\right), \forall m \in \mathcal{M}, \tag{44d}$$

$$B \sum\nolimits_{n\in N} \tau_n^m \delta_t \log_2\left(1 + \frac{\theta(\eta_u^n w_0 P_s^{nm} + \bar{P}_u^{nm} a_m^n)}{a_m^n b_m^n}\right) \geq S, \forall m \in \mathcal{M}, \tag{44e}$$

$$\sum\nolimits_{i=1}^{n} \left(E_{fly}^{nm}(\mathbf{q}) + \tau_n^m \delta_t \left(P_b + P_u^{nm}\right)\right) \leq \sum\nolimits_{i=1}^{n} \frac{\mu(1-\tau_n^m)\delta_t w_0 P_{WPT}}{a_m^n}, \forall m \in \mathcal{M}, \tag{44f}$$

$$\text{(43e), (43f)}, \tag{44g}$$

where $\Theta = \eta_u^n \omega_0 P_s^{nm}$. The problem is simplified but remains challenging to solve directly. To address this, $\mathcal{P}_{1.1}^{\mathbf{q}}$ is converted into a convex form using the following lemmas:

Lemma 2. *For each a_m^{nj} and b_m^{nj} in the jth-loop, applying the first-order Taylor approximation we get:*

$$\log_2\left(1 + \frac{e^{-E} w_0 P_s^{nm}}{a_m^n \sigma_u^2}\right) \geq \log_2\left(1 + \frac{e^{-E} w_0 P_s^{nm}}{a_m^{nj} \sigma_u^2}\right) - \frac{e^{-E} w_0 P_s^{nm} (a_m^n - a_m^{nj})}{a_m^{nj}\left(a_m^{nj}\sigma_u^2 + e^{-E} w_0 P_s^{nm}\right) ln2} \triangleq \Theta_1, \tag{45}$$

$$\log_2\left(1 + \frac{\theta(\eta_u^n \omega_0 P_s^{nm} + \bar{P}_u^{nm} a_m^n)}{a_m^n b_m^n}\right) \geq \log_2\left(1 + \theta\frac{\eta_u^n \omega_0 P_s^{nm} + \bar{P}_u^{nm} a_m^{nj}}{a_m^{nj} b_m^{nj}}\right) - \frac{\theta\eta_u^n \omega_0 P_s^{nm}(a_m^n - a_m^{nj})}{a_m^{nj}\left(\theta\eta_u^n \omega_0 P_s^{nm} + a_m^{nj}\left(\theta\bar{P}_u^{nm} + b_m^{nj}\right)\right) ln2} - \frac{\theta(\eta_u^n \omega_0 P_s^{nm} + \bar{P}_u^{nm} a_m^{nj})(b_m^n - b_m^{nj})}{b_m^{nj}\left(\theta\eta_u^n \omega_0 P_s^{nm} + a_m^{nj}\left(\theta\bar{P}_u^{nm} + b_m^{nj}\right)\right) ln2} \triangleq \Theta_2. \tag{46}$$

Proof. At any given feasible points x_j and y_j, Taylor approximation is used to approximate these convex functions [37], $\log_2\left(1 + \frac{T_1}{x}\right)$ and $\log_2\left(1 + \frac{T_2 + T_3 x}{xy}\right)(x, y \geq 0)$, individually:

$$\log_2\left(1 + \frac{T_1}{x}\right) \geq \log_2\left(1 + \frac{T_1}{x^j}\right) - \frac{T_1}{x^j\left(x^j + T_1\right)\ln 2}\left(x - x^j\right), \tag{47}$$

$$\log_2\left(1 + \frac{T_2 + T_3 x}{xy}\right) \geq \log_2\left(1 + \frac{T_2 + T_3 x^j}{x^j y^j}\right) - \frac{T_2\left(x - x^j\right)}{x^j\left(T_2 + x^j\left(T_3 + y^j\right)\right)\ln 2} - \frac{\left(T_2 + T_3 x^j\right)\left(y - y^j\right)}{y^j\left(T_2 + x^j\left(T_3 + y^j\right)\right)\ln 2}. \tag{48}$$

Applying $T_1 \triangleq e^{-E}\omega_0 P_s^{nm}$, $x \triangleq a_m^n$, $y \triangleq b_m^n$, $T_2 \triangleq \Theta\eta_u^n \omega_0 P_s^{nm}$ and $T_3 \triangleq \Theta P_u^{nm}$, we proved the Lemma 2. □

Lemma 3. *The first-order Taylor approximation is applied to each a_m^{nj} in the jth-iteration, resulting in:*

$$\frac{1}{a_m^n} \geq \frac{1}{a_m^{nj}} - \frac{1}{\left(a_m^{nj}\right)^2}\left(a_m^n - a_m^{nj}\right) \triangleq \widetilde{a}_m^n. \tag{49}$$

The formulation of $E_{fly}^{nm}(\mathbf{q})$ (11) makes the problem $\mathcal{P}_{1.1}^{\mathbf{q}}$ is still non-convex. To address this issue, a slack variable y_n^m is introduced:

$$\sqrt{{\delta_t}^4 + {k_2}^2(\Delta_n^m)^4} - k_2(\Delta_n^m)^2 \leq (y_n^m)^2, \forall n \in \mathcal{N}, \tag{50}$$

this results in a constraint:

$$\frac{\delta_n^4}{(y_n^m)^2} \leq (y_n^m)^2 + 2k_2(\Delta_n^m)^2. \tag{51}$$

This is a non-convex constraint. Applying the first-order Taylor approximation we get:

$${\delta_t}^4 \leq 2y_n^{m,j}\left(y_n^m - y_n^{m,j}\right) - 2k_2\left\|\mathbf{q}_{n+1}^{m,j} - \mathbf{q}_n^{m,j}\right\|^2 + \left(y_n^{m,j}\right)^2 + 4k_2\left(\mathbf{q}_{n+1}^{m,j} - \mathbf{q}_n^{m,j}\right)^T\left(\mathbf{q}_{n+1}^m - \mathbf{q}_n^m\right), \forall n \in \mathcal{N}, \tag{52}$$

$E_{fly}^{nm}(\mathbf{q})$ can be replaced with its upper bound $\bar{E}_{fly}^{nm}(\mathbf{q})$:

$$E_{fly}^{nm}(\mathbf{q}) \leq P_0(\delta_t + k_1(\Delta_n^m)^2) + P_1 y_n^m + \frac{k_3(\Delta_n^m)^3}{\delta_t^2} \triangleq \bar{E}_{fly}^{nm}(\mathbf{q}). \tag{53}$$

By synthesizing **Lemma 2**, **Lemma 3** and the previous manipulations, in the j-th iteration, the approximate convex problem is expressed as follows:

$$\mathcal{P}_{1.2}^{\mathbf{q}}: \underset{\mathbf{q},\mathbf{z}}{\text{maximize}}\ B\sum_{m\in\mathcal{M}}\sum_{n\in\mathcal{N}}\tau_n^m\delta_t\Theta_2 \tag{54a}$$

$$\text{s.t.}\ \ (43e),(43f),(44b),(44c), \tag{54b}$$

$$B\sum_{n\in N}\tau_n^m\delta_t\Theta_1 + \sigma S \geq B\sum_{n\in N}\tau_n^m\delta_t\Theta_2, \forall m\in\mathcal{M}, \tag{54c}$$

$$B\sum_{n\in N}\tau_n^m\delta_t\Theta_2 \geq S, \forall m\in\mathcal{M}, \tag{54d}$$

$$\frac{{\delta_t}^4}{(y_n^m)^2} \leq \left(y_n^{m,j}\right)^2 + 2y_n^{m,j}\left(y_n^m - y_n^{m,j}\right) - 2k_2\left\|\mathbf{q}_{n+1}^{m,j} - \mathbf{q}_n^{m,j}\right\|^2 + 4k_2\left(\mathbf{q}_{n+1}^{m,j} - \mathbf{q}_n^{m,j}\right)^T\left(\mathbf{q}_{n+1}^m - \mathbf{q}_n^m\right), \forall n\in\mathcal{N}, \forall m\in\mathcal{M}, \tag{54e}$$

$$\sum_{i=1}^{n}\left(\bar{E}_{fly}^{nm}(\mathbf{q}) + \tau_n^m\delta_t\left(P_b + P_u^{nm}\right)\right) \leq \sum_{i=1}^{n}\mu(1-\tau_n^m)\delta_t w_0 P_{WPT}\widetilde{a}_m^n \forall m\in\mathcal{M}. \tag{54f}$$

Standard optimization methods can directly solve $\mathcal{P}_{1.2}^{\mathbf{q}}$ since the objective and all constraints are convex [36], [38].

C. Optimize The Total Transmit Power

The objective is recalculated with optimal variables P_s^{nm}, P_u^{nm}, adhering to these constraints:

$$\mathcal{P}_1^{\mathbf{P}}: \underset{\mathbf{P}}{\text{maximize}}\ \sum\nolimits_{m\in\mathcal{M}}\sum\nolimits_{n\in\mathcal{N}}\tau_n^m\delta_t\bar{R}_d^{nm}, \tag{55a}$$

$$\text{s.t.}\ \sum\nolimits_{n\in N}\tau_n^m\delta_t\bar{R}_u^{nm} + \sigma S \geq \sum\nolimits_{n\in N}\tau_n^m\delta_t\bar{R}_d^{nm}, \forall m\in\mathcal{M}, \tag{55b}$$

$$\sum\nolimits_{n\in N}\tau_n^m\delta_t\bar{R}_d^{nm} \geq S, \forall m\in\mathcal{M}, \tag{55c}$$

$$\sum\nolimits_{i=1}^{n}\left(E_{fly}^{nm}(\mathbf{q}) + \tau_n^m\delta_t\left(P_b + P_u^{nm}\right)\right) \leq \sum_{i=1}^{n}\frac{\mu(1-\tau_n^m)\delta_t w_0 P_{WPT}}{(d_{su}^{nm})^{\alpha}}, \forall m\in\mathcal{M}, \tag{55d}$$

$$0 \leq P_u^{nm} + P_s^{nm} \leq P_{\max}, \forall m\in\mathcal{M}, \forall n\in\mathcal{N}. \tag{55e}$$

To simplify solving the optimization problem, we will transform the involved functions into convex functions with respect to the optimization variable. This transformation will be achieved through the following steps:

For ease of notation, we define $l_1^{nm} \triangleq \|\mathbf{q}_n^m - \mathbf{W}_s\|^{\alpha}$ and $l_2^{nm} \triangleq \|\mathbf{q}_n^m - \mathbf{W}_d\|^{\alpha}$.

Lemma 4. *For each $P_{s,j}^{nm}$ and $P_{u,j}^{nm}$ in the jth-loop, applying the first-order Taylor approximation we get:*

$$\log_2\left(1 + \frac{\theta P_s^{nm}}{l_1^{nm}}\right) \cong \log_2\left(1 + \frac{\theta P_{s,j}^{nm}}{l_1^{nm}}\right) + \frac{\theta(P_s^{nm} - P_{s,j}^{nm})}{\left(l_1^{nm} + \theta P_{s,j}^{nm}\right)ln2} \triangleq \widetilde{\Theta}_1, \tag{56}$$

$$\log_2\left(1 + \frac{\theta(\eta_u^n\omega_0 P_s^{nm} + \bar{P}_u^{nm} l_1^{nm})}{l_1^{nm} l_2^{nm}}\right) \cong \log_2\left(1 + \frac{\theta(\eta_u^n\omega_0 P_{s,j}^{nm} + \bar{P}_{u,j}^{nm} l_1^{nm}}{l_1^{nm} l_2^{nm}}\right) - \frac{\theta\eta_u^n\omega_0(P_s^{nm} - P_{s,j}^{nm}) + \theta l_1^{nm}\lceil\sigma\rceil(P_u^{nm} - P_{u,j}^{nm})}{(l_1^{nm} l_2^{nm} + \theta\eta_u^n\omega_0 P_{s,j}^{nm} + \theta l_1^{nm}\lceil\sigma\rceil P_{u,j}^{nm})ln2} \triangleq \widetilde{\Theta}_2. \tag{57}$$

Proof. At any given feasible points u_j and t_j, Taylor approximation is used to approximate these functions, $\log_2(1+T_1u)$ and $\log_2(1+T_2u+T_3t)(u,t\geq 0)$, individually:

$$\log_2(1+T_1u) \cong \log_2(1+T_1u_j) + \frac{T_1}{(1+T_1u_j)\ln 2}(u-u_j), \tag{58}$$

$$\log_2(1+T_2u+T_3t) \cong \log_2(1+T_2u_j+T_3t_j) + \frac{T_2(u-u_j)+T_3(t-t_j)}{(1+T_2u_j+T_3t_j)\ln 2}. \tag{59}$$

Applying $T_1 \triangleq \theta/l_1^{nm}$, $T_2 \triangleq \theta\eta\omega_0/l_1^{nm}l_2^{nm}$, $T_3 \triangleq \lceil\sigma\rceil\theta/l_2^{nm}$, $u \triangleq P_s^{nm}$, and $t \triangleq P_u^{nm}$, we proved Lemma 4. □

Applying the result from **Lemma 4**, the optimization problem is reformulated as follows:

$$\mathcal{P}_{1.1}^{\mathbf{P}}: \underset{\mathbf{P}}{\text{maximize}}\ B\sum_{m\in\mathcal{M}}\sum_{n\in\mathcal{N}}\tau_n^m\delta_t\widetilde{\Theta}_2 \tag{60a}$$

$$\text{s.t.}\ B\sum_{n\in N}\tau_n^m\delta_t\widetilde{\Theta}_1 + \sigma S \geq B\sum_{n\in N}\tau_n^m\delta_t\widetilde{\Theta}_2, \forall m\in\mathcal{M}, \tag{60b}$$

$$B\sum_{n\in N}\tau_n^m\delta_t\widetilde{\Theta}_2 \geq S, \forall m\in\mathcal{M}, \tag{60c}$$

$$\sum_{i=1}^{n}\left(E_{fly}^{nm}(\mathbf{q}) + \tau_n^m\delta_t\left(P_b + P_u^{nm}\right)\right) \leq \sum_{i=1}^{n}\frac{\mu(1-\tau_n^m)\delta_t w_0 P_{WPT}}{(d_{su}^{nm})^{\alpha}}, \forall m\in\mathcal{M}, \tag{60d}$$

$$0 \leq P_u^{nm} + P_s^{nm} \leq P_{\max} \forall m\in\mathcal{M}, \forall n\in\mathcal{N}. \tag{60e}$$

$\mathcal{P}_{1.1}^{\mathbf{P}}$ can be directly solved using standard optimization methods because the objective function and all constraints are convex [36] [38]. An iterative algorithm is proposed to achieve this goal. It relies on solving three sub-problems, and Algorithm 1 provides a summary of this alternating algorithm.

Algorithm 1 Solve problem $\mathcal{P}_1$ using efficient iterative algorithm for each UB.

Require: Set $j := 0$, $i := 0$ and initial values for $\mathbf{q}^i$, $\boldsymbol{\tau}^i$, $\mathbf{P}^j$.

repeat
  repeat
    For a given $\mathbf{q}^i$ and $\mathbf{P}^j$, the problem $\mathcal{P}_1^{\boldsymbol{\tau}}$ is solved, and the optimal solution is denoted as $\boldsymbol{\tau}^*$.
    For a given $\boldsymbol{\tau}^{i+1}$ and $\mathbf{P}^j$, the problem $\mathcal{P}_1^{\mathbf{q}}$ is solved, and the optimal solution is denoted as $\mathbf{q}^*$.
    Update the local point $\boldsymbol{\tau}^{i+1} = \boldsymbol{\tau}^*$ and $\mathbf{q}^{i+1} = \mathbf{q}^*$.
    Set $i := i + 1$.
  until Convergence with $\epsilon > 0$.
  For a given $\mathbf{q}^*$ and $\boldsymbol{\tau}^*$, the problem $\mathcal{P}_1^{\mathbf{P}}$ is solved, and the optimal solution is denoted as $\mathbf{P}^*$.
  Update the local point $\mathbf{P}^{j+1} = \mathbf{P}^*$.
  Set $j := j + 1$.
until Convergence with $\epsilon > 0$.

D. Complexity Analysis

We provide an in-depth complexity analysis of Algorithm 1. The proposed closed-form expressions efficiently address the problem $\mathcal{P}1^{\boldsymbol{\tau}}$, thereby resolving $\mathcal{P}1^{\mathbf{q}}$ and $\mathcal{P}1^{\mathbf{P}}$ as the primary subproblems in this context. Given that $\mathcal{P}1^{\mathbf{q}}$ exhibits a logarithmic structure, its complexity is determined as $\mathcal{O}\left(L_1\left(3N\right)^{3.5}\right)$, where L_1 is the number of iterations required to update the UBD trajectory, and $3N$ denotes the number of scalar variables involved [39]. Therefore, the overall computational complexity of $\mathcal{P}1^{\mathbf{q}}$ and $\mathcal{P}1^{\boldsymbol{\tau}}$ is $\mathcal{O}\left(L_2 L_1\left(3N\right)^{3.5}\right)$, where L_2 is the number of iterations needed for convergence to be achieved. Similarly, the complexity associated with solving $\mathcal{P}1^{\mathbf{q}}$ and $\mathcal{P}_1^{\mathbf{P}}$ is $\mathcal{O}\left(L_3\left(3N\right)^{3.5}\right)$, where L_3 represents the iterations required to update the transmit power and $3N$ corresponds to the number of scalar variables. Thus, the total complexity of Algorithm 1 amounts to $\mathcal{O}\left(L_4\left(3N\right)^{3.5}\left(L_1 L_2 + L_3\right)\right)$, where L_4 is the number of iterations essential for convergence in this comprehensive case.

IV. Evolutionary-based solution

An Evolutionary Algorithm is a type of optimization algorithm that employs strategies inspired by biological evolution, such as mutation, recombination, and natural selection. The goal is to identify the optimal configuration for a system within given constraints. We present the Genetic Algorithm (GA) to solve the problem $\mathcal{P}_1$. The algorithm begins by initializing a population of individuals and maintains this population throughout the search process. In each generation, pair of individuals undergo crossover to create two new offstrings, which are then subjected to mutation. These offspring are evaluated and selected for the next generation based on their fitness. The ultimate goal of the problem is to maximize the total data transmission of each UBD from the source to the destination and is formulated as (29a).

A. Solution Representation

The variables of the problem are the coordinates in 3D space $(x, y, z)^{nm}$, $\tau_n^m, P_u^{nm}, P_s^{nm}$. Here, q_n^m represents the position of a UBD at time slot n, and its position is defined by the coordinates $(x, y, z)^{nm}$. We have $N = T/\,\delta_t$ time slots, and in of these time slots, the values of $(x, y, z)^{nm}$, τ_n^m, P_u^{nm}, and P_s^{nm} vary. Therefore, each UBD is a population $\mathcal{Q}$ consisting of $\mathbf{I}$ individuals, where each individual is a $6 \times N$-dimensional vector $c = \{c_1, c_2, \ldots, c_{6\times N}\}$ of real numbers in the range $(0, 1)$, representing the parameters of the problem at each time slot. To translate these values into real-world parameters, we multiply them by specific scaling factors chosen during the algorithm setup. Specifically,

1) Representing the coordinates $(x, y, z)^{nm}$ at n-th time slots into the actual coordinates we get
$$x^{nm} = \{c_1, c_2, \ldots, c_N\} \times X, \tag{61}$$
$$y^{nm} = \{c_{N+1}, c_{N+2}, \ldots, c_{2N}\} \times Y, \tag{62}$$
$$z^{nm} = \{c_{2N+1}, c_{2N+2}, \ldots, c_{3N}\} \times Z, \tag{63}$$
where X, Y, Z are the limit values of (x, y, z) coordinates in 3D space.
2) We can also do the same for τ_n^m, P_u^{nm}, P_s^{nm} as follows
$$\tau_n^m = \{c_{3N+1}, c_{3N+2}, \ldots, c_{4N}\} \times t, \tag{64}$$
$$P_u^{nm} = \{c_{4N+1}, c_{4N+2}, \ldots, c_{5N}\} \times P_U, \tag{65}$$
$$P_s^{nm} = \{c_{5N+1}, c_{5N+2}, \ldots, c_{6N}\} \times P_S. \tag{66}$$
Here, t, P_U and P_S are the limit values for τ_n^m, P_u^{nm} and P_s^{nm}.

B. The Fitness Function

Before initializing the initial population, we define the fitness function $Fitness(c)_m$ of the m-th UBD.

$$Fitness(c)_m = \max \sum_{n=1}^{N} \tau_n^m \log_2\left(1 + \frac{\theta(n_u w_0 P_s^{nm} + \bar{P}_u^{nm} d_{su}^{nm})}{(d_{su}^{nm})^{\alpha}(d_{du}^{nm})^{\alpha}}\right) \tag{67}$$

Each individual within the population is assessed using the fitness function to determine its suitability. Individuals with higher fitness values are more likely to be selected for the next generation. According to the problem's objective, the function evaluates the solution to $\mathcal{P}_1$. However, for an individual in the population to be feasible, it must satisfy the following constraints:

1) The distance the UBD travels between two consecutive time slots n and $n + 1$ must be less than the maximum distance the UBD can fly, as defined by (29f) (29g).
2) The total flying energy of the UBD E_{fly}^{nm} must be less than the total energy harvested, E_h^{nm}, (29d).
3) The data transmission rate received at the destination must exceed the transmission rate of the UBD (29b).
4) Finally, the data transmission rate received at the destination must be greater than the minimum transmission rate at the destination S, to ensure technical requirements and user needs (29c).

If an individual c fails to satisfy the first three constraints, the result of the evaluation function $Fitness(c)_m$ = 0. However, if it meets the first three constraints but fails the last one, the fitness value of this individual will be penalized with a penalty factor depending on the requirements of the problem.

$$Fitness(c)_m = p \times Fitness(c)_m, \tag{68}$$

where p is a penalty factor in the range of $(0, 1)$. To enforce the constraint (29e), $0 \leq P_u^{nm} + P_s^{nm} \leq P_{\max}$, we restrict the values of P_u^{nm} and P_s^{nm} from the outset of the algorithm. As explained, P_u^n and P_s^n for the n-th time slots are expressed as real numbers within the range of $(0, 1)$.

Accordingly, we establish the initial constraints for P_u^{nm}, P_s^{nm} based on the specified $P_{\max}$. Nevertheless, due to the UBD's limitation, P_u^{nm} cannot exceed P_s^{nm}, necessitating an additional restriction on P_u^{nm}. To clarify, in this context,

$$P_u^{nm} = \{c_{4N+1}, c_{4N+2}, \ldots, c_{5N}\} \times P_U, \tag{69}$$

$$P_U \leq P_U^*, \tag{70}$$

$$P_s^{nm} = \{c_{5N+1}, c_{5N+2}, \ldots, c_{6N}\} \times P_S. \tag{71}$$

Here, P_U and P_S serve as the limit values to satisfy the aforementioned constraint. Additionally, P_U^* is the upper limit imposed to restrict the value of P_U.

C. Population Initialization

In the population initializing step, we aim to generate individuals randomly. Every individual in the population is represented by a gene sequence that signifies a potential solution to the problem. The population size is predefined and significantly impacts the performance of the genetic algorithm. The diversity of the initial population is crucial to ensure that the algorithm can explore the entire solution space and avoid local optima. During the initialization of each individual, every randomly generated individual is evaluated through the fitness function. Specifically, if

$$\text{Fitness}(c_i)_m > 0, \forall i \in \{0, ..., I\} \tag{72}$$

then c_i is added to the population. Otherwise, the candidate is eliminated. To enhance the efficiency of creating suitable individuals, we incorporate initial constraints (11) and (29f) into the initialization process.

D. Crossover

Crossover is the process of combining two individuals (parents) to generate one or more offspring. This process mimics natural reproduction, where genes from both parents are merged to produce offspring with genetic traits from both sides. Crossover introduces diversity into the population and aids in exploring new solutions. After initializing the initial population, the process of creating a new generation begins. First, we randomly select two individuals from the current population to serve as the parent individuals for the crossover process. We utilize crossover for binary arrays, specifically one-point crossover, to combine two parent individuals, fa and mo, to create two offspring c_1 and c_2:

$$c_1 = u.fa + (1 - u)mo, \tag{73}$$

$$c_2 = (1 - u)fa + u.mo, \tag{74}$$

where u is a real number in the range (0,1) representing the crossover point. This process is repeated $I/2$ times to generate a sub-population Q' consisting of individuals, with the total number of individuals in Q' equal to I.

Algorithm 2 Solve problem $\mathcal{P}_1$ using GA for UBDs.

1: Start by randomly initializing the initial population, denoted as Q and I individuals.
2: Evaluate the fitness of each individual in the population using the predefined fitness function $Fitness(c)$.
3: Set the maximum of generations $G_{\max}$ and initialize $G \leftarrow 0$.
4: **for** $G \leftarrow 0$ to $G_{\max}$ **do**
5: Select parents from the initial population, Q.
6: Perform crossover to create a new population, Q'.
7: Apply mutation to the individuals in population Q'.
8: Combine population Q' with the initial population Q, forming Q". Calculate the fitness of the individuals in Q", arranging them in descending order.
9: Select 50% of the individuals from population Q" to create a new population for the next iteration.
10: **end for**

E. Mutation

Mutation involves the random alteration of one or more genes within an individual. This process simulates natural mutations, facilitating the creation of new traits and maintaining genetic diversity within the population. After crossover, a population Q' is obtained. With the number of mutated individuals denoted as I_1, the individuals in population Q' undergo mutation via replacement mutation process as follows:

$$I_1 = I\theta, \tag{75}$$

where θ is the mutation coefficient. These individuals are mutated by selecting any position and replacing it with a random number in the range $[0, 1)$.

F. Selection

Following the creation of offspring through crossover and mutation, these individuals are evaluated and selected to form the next generation. After mutation, we merge the population Q' with Q to create a population Q" consisting of $2I$ individuals. According to the original design of the algorithm, only I individuals are retained in the population.

We rely on the fitness function to sort the individuals of Q" in descending order. Then we employ a hierarchical selection based on the fitness function to retain half the number of individuals. Specifically, we select $40\%I$ of the best individuals, $40\%I$ of the average individuals, and $20\%I$ of the worst individuals. An overview of this evolutionary algorithm can be found in Algorithm 2.

G. Complexity Analysis

We now present the complexity analysis of Algorithm 2. Genetic Algorithms are stochastic, and their complexity depends on the genetic operators, their implementation, the representation of the individuals and the population, and the fitness function. Therefore, the complexity of Genetic Algorithms is $\mathcal{O}(6NPG_{\max}))$, where $G_{\max}$ is the number of generations, P is the population size, and $6N$ is the size of the individuals.

TABLE II
SIMULATION PARAMETERS

Parameters	Values
Maximum speed of UB, V_{max}	20 $\frac{m}{s}$
Power noise, σ^2	-90 dB
Path loss exponent, α	2.3
Total flight time of the UB, T	50 s
Backscatter power, P_b	1 μW
System bandwidth, B	1 MHz
channel power gain at reference distance, ω_o	-30 dB
Duration of one time slot, δ_t	0.5 s
Energy harvesting coefficient, μ	0.84
Backscatter coefficient, η	0.5
Data demanded, S	50 Mbits
Maximum allowable total transmit power, $P_{\max}$	60 mW
Optimization threshold, ϵ	10^{-4}

V. Numerical Results

This section presents the numerical results validating the performance of the proposed scheme. It is assumed that the source and destination are located at $\mathbf{W}_s = [5, 0, 0]^T$ and $\mathbf{W}_d = [15, 0, 0]^T$. To improve readability and ease intuitive understanding of the collected data, this analysis is limited to two UBDs, denoted as UAV_1 and UAV_2. The initial and final points of the UAV_1 are denoted by $\mathbf{q}_I^1 = [0, 10, 10]^T$ and $\mathbf{q}_F^1 = [20, 10, 10]^T$, respectively. For UAV_2, $\mathbf{q}_I^2 = [0, 10, 5]^T$ and $\mathbf{q}_I^2 = [20, 10, 10]^T$ designate its initial and final points, respectively. In this study, the value of σ is set to 0.35, indicating that each UBD stores a segment of the data equivalent to 35% of the total amount transmitted by the source. Source S's initial transmit power to each UBD and UBD's initial transmit power are set at $\mathbf{P}_s = 16$ dBm and $\mathbf{P}_u = 5$ mW, respectively. Furthermore, a power level of $P_{WPT} \in [27, 40]$ [40] is designated for source S during WPT. The remaining parameters are shown specifically in Table II. The efficacy of the proposed algorithms is evaluated against various benchmark schemes, which are detailed below:

- Complete(Com): Using **Algorithm 1** to solve the problem.
- 3D+OP: Similar to **Algorithm 1** but for only 1 UB.
- 2D+2UAV: Similar to **Algorithm 1** but does not optimize the transmit power and fix the flight trajectory height of the UBDs at height H.

Fig. 2 illustrates the trajectories of UAV_1 and UAV_2 derived using the proposed **Algorithm 1**. To ensure practicality in real-world implementations, the UBD trajectories are carefully designed such that they always maintain a minimum altitude of at least 3 meters. This minimum threshold ensures compliance with safe operational parameters for UAVs in diverse environments. Each UBD commences its journey from an initial point, transitions to a position near the line connecting the source and destination, and then concludes at its designated final point. During this movement, the UBDs typically descend to the lowest allowable altitude and follow a trajectory around a strategically chosen location situated on the direct line between the source and the destination. This strategy minimizes the distances between the source and the UBD and between the UBD and the destination, thereby enhancing both energy collection and data transmission efficiency. Notably, the location around

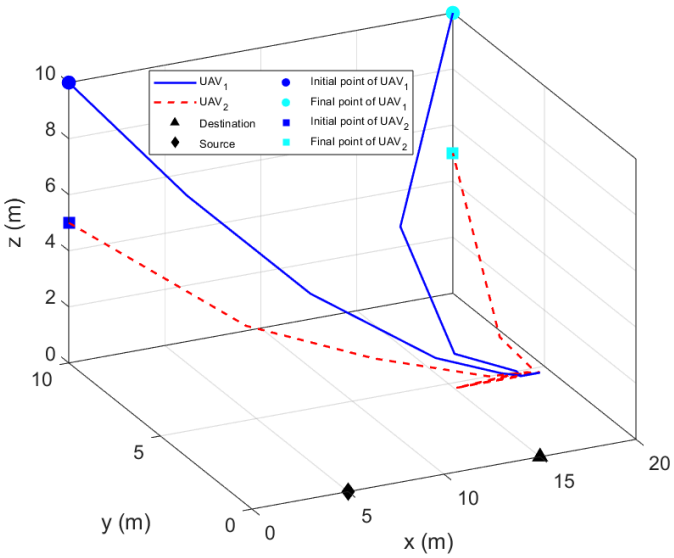

Fig. 2. The optimized trajectory of the two UAVs.

which the UBDs orbit is influenced by the value of P_{WPT} [37], which dynamically adjusts the UBDs' paths to improve energy transfer while maximizing overall throughput.

Fig. 3(a) examines the relationship between the required data size S, expressed in bits, and the overall throughput performance of the UAV network. The simulations were conducted with fixed parameters, including $T = 30$ seconds, $P_{WPT} = 10^4$ W, $V_{\max} = 20$ m/s, $\mathbf{P}_s = 15$ mW, $P_{\max} = 20$ mW, and an initial reflection time $\boldsymbol{\tau} = 0.4$. For the proposed optimization method, the reflection time ratio σ is set to 0.45, whereas for the 3D+OP approach, it is assigned a value of 0.9. The 2D+2UAV scenario employs a constant altitude of $H = 5$ meters for all trajectories. Results highlight that the proposed BCD algorithm achieves a significantly higher throughput than alternative methods. Specifically, with a data demand of $S = 70$ Mbits, the throughput reaches 324.75 Mbits, compared to 210.24 Mbits and 316.12 Mbits for the 3D+OP and 2D+2UAV methods, respectively. These gains are attributed to the efficient use of available resources, including transmission power P_s, total travel time T, and optimized reflection time τ_n, underscoring the algorithm's superiority in resource allocation.

Fig. 3(b) illustrates how throughput performance varies with changes in source charging power P_{WPT}. The simulation parameters include a travel time of $T = 30$ seconds, source power $\mathbf{P}_s = 10$ mW, data size $S = 20$ Mbits, and maximum power $P_{\max} = 15$ mW. For the proposed algorithm, the reflection time ratio σ is maintained at 0.45, while for the 3D+OP method, it is configured as 0.9. The results show that the proposed Com strategy consistently achieves the highest throughput across all tested power levels. For instance, when $P_{WPT} = 30$ dB, the throughput values for the Com, 2D+2UAV, and 3D+OP strategies are 162.29 Mbits, 157.2 Mbits, and 136.12 Mbits, respectively. These findings emphasize the ability of the proposed method to optimize energy utilization effectively, outperforming benchmarks under various power configurations and further validating its applicability in energy-limited scenarios.

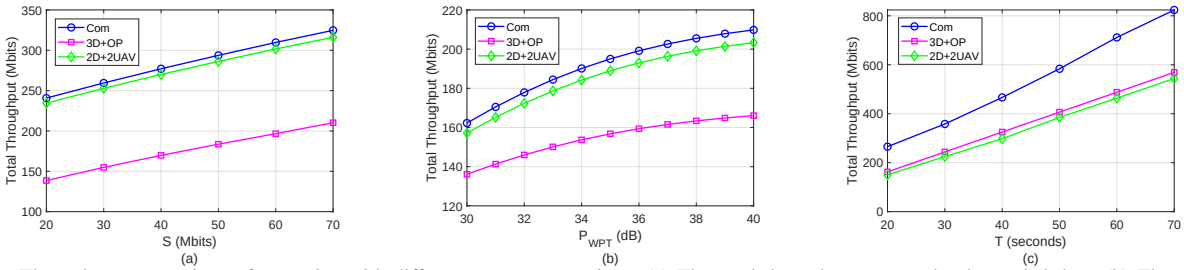

Fig. 3. Throughput comparison of scenarios with different parameter settings: (a) The total throughput versus the demanded data. (b) The total throughput versus P_{WPT}. (c) The total throughput versus traveling time T.

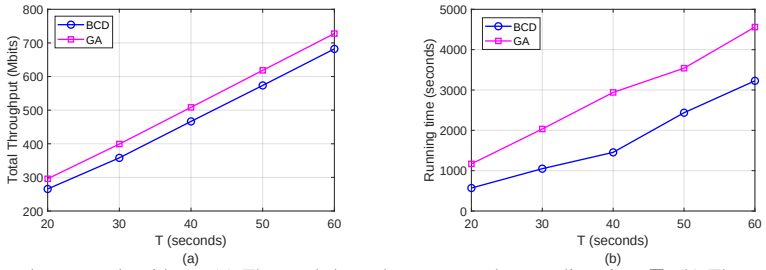

Fig. 4. Performance comparison between algorithms: (a) The total throughput versus the traveling time T. (b) The running time versus the traveling time T.

Fig. 3(c) delves into the impact of total travel time on performance metrics, with $P_{WPT} = 10^4$ W, $S = 70$ Mbits, $\delta_t = 0.5$ s and $P_{\max} = 60$ mW. We set $\sigma = 0.45$ for the proposed method and $\sigma = 0.9$ for 3D+OP. The altitude of the UBDs is fixed at $H = 10$ m in the 2D+2UAV method. All algorithms exhibit an increasing trend in total throughput as the travel time T (seconds) increases. This is consistent with equation (29a), which predicts that the total gathered throughput at the destination scales proportionately with reflection time. The findings show that the proposed algorithm significantly outperforms the benchmarks in terms of overall throughput (bps). Notably, the proposed algorithm achieves a maximum throughput of 180.52 Mbps with a travel time of $T = 100$ seconds, whereas the throughput of the 3D+OP and 3D+2UAV schemes is limited to 119.541905 Mbps and 96.601535 Mbps, respectively. This demonstrates the effectiveness of our approach over the benchmarks that do not utilize multiple UBDs or optimize total transmit power.

Under the constraints $V_{\max} = 20$ m/s, $\mathbf{P}_s = 16$ dBm, data size $S = 70$ Mbits, and $P_{\max} = 60$ mW, the Genetic Algorithm (GA) initializes with a population of 100 individuals, a mutation rate of 0.1, and up to 10,000 generations. Fig. 4(a) presents a comparative analysis of total throughput for the GA and BCD algorithms based on total movement time. GA demonstrates a consistent advantage, achieving marginally higher throughput than BCD. For instance, with movement times of 40 and 60 seconds, the GA yields throughputs of 508.36 Mbits and 727.85 Mbits, respectively, representing increases of 7.9% and 6.2% over BCD. These outcomes underscore the potential of GA to optimize throughput effectively through evolutionary computation techniques, albeit at a higher computational cost.

Fig. 4(b) illustrates the total computational time for both proposed algorithms. It can be observed that the computational time for both methods increases significantly with the increase in flight time T. For example, when the UB movement time is 30, 40, and 50 seconds, the computation time for the BCD method is 1049, 1453, and 2436 seconds, respectively. Furthermore, the computational time for the GA method is considerably higher than that of BCD. For instance, when T is 50 and 60 seconds, the GA takes 31.19% and 29.23% longer than BCD, respectively. This can be attributed to the fact that the complexity of the BCD method mainly depends on the optimization of the trajectory and transmission power, as closed-form expressions can be obtained for the optimal DTS values. This leads to a significant reduction in computational time for BCD. In contrast, the GA method requires calculating all the fitness values for a large number of individuals and generations in each iteration, which increases its complexity compared to BCD. Based on the observations in Fig. 4(a) and Fig. 4(b), the advantages and drawbacks of both the BCD and GA algorithms are evident, with respect to their performance in total throughput and computational time in solving optimization problems.

VI. Conclusions

This study presents a novel network architecture tailored to ensure reliable service provision to destinations, even in the absence of a direct communication link. The proposed framework capitalizes on the combined application of caching and backscatter technologies integrated with multiple UBDs operating within a three-dimensional environment, resulting in notable enhancements in system efficiency. A joint optimization strategy is adopted to simultaneously fine-tune the DTS ratio, UBD trajectories, and transmission power, thereby maximizing the total network throughput. Simulation outcomes reveal that the suggested methods deliver superior performance compared to conventional reference frameworks in terms of overall throughput. These results emphasize the design's effectiveness, especially in scenarios lacking multiple UBDs or optimized total transmission power configurations. Additionally, comparative analyses demonstrate the distinct advantages of both the BCD-based optimization technique and the Genetic Algorithm, highlighting their individual strengths in addressing complex optimization challenges. Future inves-

tigations will explore the nuanced trade-off between energy harvesting and data transmission durations, focusing on dynamic adaptations to further advance system efficiency and overall performance metrics.

REFERENCES

[1] K. Teixeira, G. Miguel, H. S. Silva, and F. Madeiro, "A survey on applications of unmanned aerial vehicles using machine learning," *IEEE Access*, vol. 11, pp. 117 582–117 621, 2023.

[2] J. Pietz, J. H. Wilck, S. Christensen, M. Melville, J. Q. Stank, and S. Zaiser, "Autonomous target search using unmanned aerial vehicles in the presence of signal noise," *IEEE Communications Letters*, vol. 26, no. 9, pp. 2141–2145, 2022.

[3] J. Zhang, J. Cui, H. Zhong, I. Bolodurina, and L. Liu, "Intelligent drone-assisted anonymous authentication and key agreement for 5g/b5g vehicular ad-hoc networks," *IEEE Transactions on Network Science and Engineering*, vol. 8, no. 4, pp. 2982–2994, 2021.

[4] A. Gao, Z. Shao, Y. Hu, and W. Liang, "Joint trajectory and energy efficiency optimization for multi-uav assisted offloading," in *IGARSS 2022 - 2022 IEEE International Geoscience and Remote Sensing Symposium*, 2022, pp. 508–511.

[5] Z. Na, C. Ji, B. Lin, and N. Zhang, "Joint optimization of trajectory and resource allocation in secure uav relaying communications for internet of things," *IEEE Internet of Things Journal*, vol. 9, no. 17, pp. 16 284–16 296, 2022.

[6] A. Mondal, D. Mishra, G. Prasad, and A. Hossain, "Joint optimization framework for minimization of device energy consumption in transmission rate constrained uav-assisted iot network," *IEEE Internet of Things Journal*, vol. 9, no. 12, pp. 9591–9607, 2022.

[7] A. Kumar and B. Singh, "Irs-assisted laser-powered uav energy harvesting for iot networks," *IEEE Internet of Things Journal*, vol. 11, no. 5, pp. 7890–7901, 2024.

[8] M. A. Jamshed and F. Ayaz, "Green uav-enabled internet-of-things network with ai-assisted noma for disaster management," *IEEE Internet of Things Journal*, vol. 10, no. 17, pp. 6500–6514, 2023.

[9] H. Luo, Q. Zhang, H. Yu, G. Sun, and S. Xu, "Symbiotic pbft consensus: Cognitive backscatter communications-enabled wireless pbft consensus," in *GLOBECOM 2023 - 2023 IEEE Global Communications Conference*, 2023, pp. 910–915.

[10] X. Zhang, W. Liu, N. Huang, and Z. Xu, "Backscattering interference channel characteristics in full-duplex underwater optical wireless communication," in *2023 15th International Conference on Communication Software and Networks (ICCSN)*, 2023, pp. 326–330.

[11] S. Sood, "An overview of backscatter communication technique for performing wireless sensing in green communication networks," in *2023 International Conference on Power Energy, Environment & Intelligent Control (PEEIC)*, 2023, pp. 7–11.

[12] G. Yang, R. Dai, and Y.-C. Liang, "Energy-efficient uav backscatter communication with joint trajectory design and resource optimization," *IEEE Transactions on Wireless Communications*, vol. 20, no. 2, pp. 926–941, 2021.

[13] W. Lu, Y. Ding, Y. Gao, S. Hu, Y. Wu, N. Zhao, and Y. Gong, "Resource and trajectory optimization for secure communications in dual unmanned aerial vehicle mobile edge computing systems," *IEEE Transactions on Industrial Informatics*, vol. 18, no. 4, pp. 2704–2713, 2022.

[14] Z. Guan, S. Wang, L. Gao, and W. Xu, "Energy-efficient uav communication with 3d trajectory optimization," in *2021 7th International Conference on Computer and Communications (ICCC)*, 2021, pp. 312–317.

[15] H. Tian, M. Yan, L. Dai, and P. Yang, "Joint communication and computation resource scheduling of a solar-powered uav-assisted communication system for platooning vehicles," in *2023 9th International Conference on Mechanical and Electronics Engineering (ICMEE)*, 2023, pp. 49–54.

[16] L. Xie, X. Cao, J. Xu, and R. Zhang, "Uav-enabled wireless power transfer: A tutorial overview," *IEEE Transactions on Green Communications and Networking*, vol. 5, no. 4, pp. 2042–2064, 2021.

[17] Y. Liu, K. Xiong, Y. Lu, Q. Ni, P. Fan, and K. B. Letaief, "Uav-aided wireless power transfer and data collection in rician fading," *IEEE Journal on Selected Areas in Communications*, vol. 39, no. 10, pp. 3097–3113, 2021.

[18] H. Ren, Z. Zhang, Z. Peng, L. Li, and C. Pan, "Energy minimization in ris-assisted uav-enabled wireless power transfer systems," *IEEE Internet of Things Journal*, vol. 10, no. 7, pp. 5794–5809, 2023.

[19] D. N. K. Jayakody, T. D. P. Perera, A. Ghrayeb, and M. O. Hasna, "Self-energized uav-assisted scheme for cooperative wireless relay networks," *IEEE Transactions on Vehicular Technology*, vol. 69, no. 1, pp. 578–592, 2020.

[20] H. Yan, Y. Chen, and S.-H. Yang, "Uav-enabled wireless power transfer with base station charging and uav power consumption," *IEEE Transactions on Vehicular Technology*, vol. 69, no. 11, pp. 12 883–12 896, 2020.

[21] M. Sheng, J. Liu, R. Zhang, G. Li, and W. Xu, "Uav-assisted mobile edge computing with backscatter-aided iot devices: Task scheduling and resource allocation," *IEEE Internet of Things Journal*, vol. 10, no. 6, pp. 4942–4955, 2023.

[22] F. Fazel, J. Abouei, M. Jaseemuddin, A. Anpalagan, and K. N. Plataniotis, "Secure throughput optimization for cache-enabled multi-uavs networks," *IEEE Internet of Things Journal*, vol. 9, no. 10, pp. 7783–7801, 2022.

[23] Y. Liu, C. Yang, X. Chen, and F. Wu, "Joint hybrid caching and replacement scheme for uav-assisted vehicular edge computing networks," *IEEE Transactions on Intelligent Vehicles*, vol. 9, no. 1, pp. 866–878, 2024.

[24] A. Masood, T.-V. Nguyen, T. P. Truong, and S. Cho, "Content caching in hap-assisted multi-uav networks using hierarchical federated learning," in *2021 International Conference on Information and Communication Technology Convergence (ICTC)*, 2021, pp. 1160–1162.

[25] R. Zhang, R. Lu, X. Cheng, N. Wang, and L. Yang, "A uav-enabled data dissemination protocol with proactive caching and file sharing in v2x networks," *IEEE Transactions on Communications*, vol. 69, no. 6, pp. 3930–3942, 2021.

[26] Z. Zhao, X. Zhang, H. Li, K. Deng, and K. Wu, "Joint cooperative caching and power control for uav-enabled vehicular iot networks," *IEEE Internet of Things Journal*, vol. 11, no. 3, pp. 2190–2204, 2024.

[27] M. Hua, L. Yang, C. Li, Q. Wu, and A. L. Swindlehurst, "Throughput maximization for uav-aided backscatter communication networks," *IEEE Transactions on Communications*, vol. 68, no. 2, pp. 1254–1270, 2020.

[28] Y. Yuan, L. Lei, T. X. Vu, S. Chatzinotas, S. Sun, and B. Ottersten, "Energy minimization in uav-aided networks: Actor-critic learning for constrained scheduling optimization," *IEEE Transactions on Vehicular Technology*, vol. 70, no. 5, pp. 5028–5042, 2021.

[29] B. Lyu, C. You, Z. Yang, and G. Gui, "The optimal control policy for rf-powered backscatter communication networks," *IEEE Transactions on Vehicular Technology*, vol. 67, no. 3, pp. 2804–2808, 2018.

[30] Y. Zeng, J. Xu, and R. Zhang, "Energy minimization for wireless communication with rotary-wing uav," *IEEE Transactions on Wireless Communications*, vol. 18, no. 4, pp. 2329–2345, 2019.

[31] S. Xiao, H. Guo, and Y.-C. Liang, "Resource allocation for full-duplex-enabled cognitive backscatter networks," *IEEE Transactions on Wireless Communications*, vol. 18, no. 6, pp. 3222–3235, 2019.

[32] X. Kang, Y.-C. Liang, and J. Yang, "Riding on the primary: A new spectrum sharing paradigm for wireless-powered iot devices," *IEEE Transactions on Wireless Communications*, vol. 17, no. 9, pp. 6335–6347, 2018.

[33] S. Gong, X. Huang, J. Xu, W. Liu, P. Wang, and D. Niyato, "Backscatter relay communications powered by wireless energy beamforming," *IEEE Transactions on Communications*, vol. 66, no. 7, pp. 3187–3200, 2018.

[34] I. S. Gradshteyn and I. M. Ryzhik, *Table of integrals, series, and products*. Academic press, 2014.

[35] M. Hong, M. Razaviyayn, Z.-Q. Luo, and J.-S. Pang, "A unified algorithmic framework for block-structured optimization involving big data: With applications in machine learning and signal processing," *IEEE Signal Processing Magazine*, vol. 33, no. 1, pp. 57–77, 2016.

[36] S. P. Boyd and L. Vandenberghe, *Convex optimization*. Cambridge university press, 2004.

[37] D.-H. Tran, S. Chatzinotas, and B. Ottersten, "Throughput maximization for backscatter- and cache-assisted wireless powered uav technology," *IEEE Transactions on Vehicular Technology*, vol. 71, no. 5, pp. 5187–5202, 2022.

[38] S. Boyd, "Advances in convex optimization: Interior-point methods, cone programming, and applications," in *Proc. 41st IEEE Conf. Decis. Control*, vol. 4, 2002.

[39] G. Zhang, Q. Wu, M. Cui, and R. Zhang, "Securing uav communications via joint trajectory and power control," *IEEE Transactions on Wireless Communications*, vol. 18, no. 2, pp. 1376–1389, 2019.

[40] S. Yin, L. Li, and F. R. Yu, "Resource allocation and basestation placement in downlink cellular networks assisted by multiple wireless powered uavs," *IEEE Transactions on Vehicular Technology*, vol. 69, no. 2, pp. 2171–2184, 2020.